Label-free Her2 detection and dissociation constant assessment in diluted human serum using a longitudinal extension mode of a piezoelectric microcantilever sensor

Joseph A. Capobianco[a], Wan Y. Shih[b],*, Gregory P. Adams[c], Wei-Heng Shih[a]

[a] Department of Materials Science and Engineering, Drexel University, Philadelphia, PA 19104, United States
[b] School of Biomedical Engineering, Science, and Health Systems, Drexel University, Philadelphia, PA 19104, United States
[c] Developmental Therapeutics Program, Fox Chase Cancer Center, Philadelphia, PA, United States

ABSTRACT

We have investigated real-time, label-free, in situ detection of human epidermal growth factor receptor 2 (Her2) in diluted serum using the first longitudinal extension mode of a lead zirconate-lead titanate (PZT)/glass piezoelectric microcantilever sensor (PEMS) with H3 single-chain variable fragment (scFv) immobilized on the 3-mercaptopropyltrimethoxysilane (MPS) insulation layer of the PEMS surface. We showed that with the longitudinal extension mode, the PZT/glass PEMS consisting of a 1 mm long and 127 μm thick PZT layer bonded with a 75 μm thick glass layer with a 1.8 mm long glass tip could detect Her2 at a concentration of 6–60 ng/ml (or 0.06–0.6 nM) in diluted human serum, about 100 times lower than the concentration limit obtained using the lower-frequency flexural mode of a similar PZT/glass PEMS. We further showed that with the longitudinal mode, the PZT/glass PEMS determined the equilibrium H3–Her2 dissociation constant K_d to be $3.3 \pm 0.3 \times 10^{-8}$ M consistent with the value, $3.2 \pm 0.28 \times 10^{-8}$ M deduced by the surface plasmon resonance method (BIAcore).

© 2011 Elsevier B.V. All rights reserved.

1. Introduction

Human epidermal growth factor receptor 2 (Her2) is a cancer antigen that can be measured and evaluated as an indicator for normal biologic processes, pathogenic processes, or pharmacologic responses to therapeutic intervention. Specifically, the Her2 proto-oncogene is amplified and/or overexpressed in approximately 20–25% of invasive breast cancers [1]. The extracellular domain (ECD) of the Her2 protein is often cleaved and released into the circulation with serum concentrations elevated in 20–50% of patients with primary breast cancer and 50–62% of metastatic disease [2,3]. Normal individuals have a Her2 concentration between 2 and 15 ng/ml in the blood and breast cancer patients have blood Her2 levels from 15 to 75 ng/ml [4]. The screening of Her2 on tumor biopsies is often used to evaluate whether a patient may successfully respond to therapy with trastuzumab (Herceptin), a monoclonal anti-Her2 antibody.

Piezoelectric microcantilever sensors (PEMS) consisting of a highly piezoelectric layer bonded to a nonpiezoelectric layer are a new type of biosensors whose mechanical resonance can both be excited and detected by electrical means. Most of the earlier

PEMS detection studies involved low-frequency flexural (bending)-mode resonance. A schematic of the first-mode flexural vibration is shown by Fig. 1(a). With receptors immobilized on the PEMS surface, binding of antigens shifts the PEMS flexural resonance frequency. Real-time, label-free antigen detection is achieved by electrically monitoring the PEMS flexural resonance frequency shift [5–12]. Detection sensitivity of PEMS flexural resonance is strongly affected by the size and the thickness of the PEMS [13–15]. The mass sensitivity defined as $-\Delta f/\Delta m$ increased dramatically with a reduced PEMS size and/or thickness [13] where Δf and Δm are the PEMS detection resonance frequency shift and the corresponding mass change due to the binding of antigens on the sensor surface. For a lead zirconate titanate (PZT)/glass PEMS about 1 mm long consisting of a 127 μm commercial PZT layer on a 75–150 μm glass layer with a 2 mm long glass tip its mass detection sensitivity was on the order of 10^{10} Hz/g [5–8,10,11]. Whereas for a lead magnesium niobate-lead titanate, $(PbMg_{1/3}Nb_{2/3}O_3)_{0.63}$–$(PbTiO_3)_{0.37}$ (PMN-PT)/tin PEMS 600–1200 μm long consisting of an 8 μm thick PMN-PT layer bonded with a 5 μm thick tin layer its mass detection sensitivity on the order of 10^{12}–10^{13} Hz/g [8–11]. A PZT/SiO$_2$ 60 μm long consisting of a 1 μm thick PZT thin film on 1 μm thick SiO$_2$ layer with a 20 μm long SiO$_2$ tip exhibited a mass sensitivity of 10^{16} Hz/g [16].

As a result of the thickness and size differences earlier Her2 detection studies showed a dramatic difference in concentration

* Corresponding author. Tel.: +1 215 895 2325; fax: +1 215 895 4983.
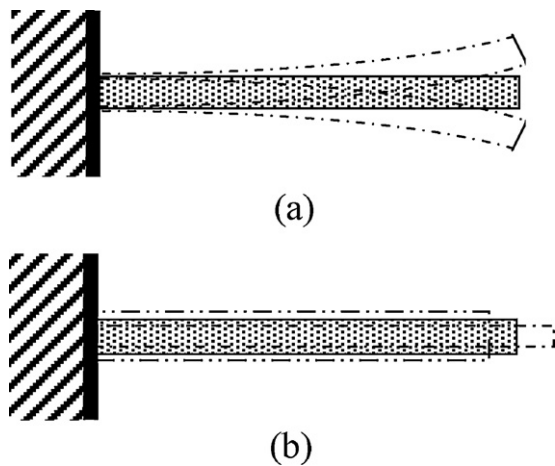E-mail address: shihwy@drexel.edu (W.Y. Shih).

Fig. 1. (a) A schematic of the first bending mode vibration where the shaded bar illustrated the initial position of the PEMS and the dash-dotted shapes illustrate the bent positions, and (b) a schematic of the first longitudinal mode vibration where the shaded bar illustrated the initial position of the PEMS and the dash-dotted shapes illustrate the extended or contracted positions.

sensitivities between the PMN-PT PEMS and the PZT/glass PEMS [11]: A 127-μm thick PZT/glass PEMS exhibited only a μg/ml concentration sensitivity while an 8-μm thick PMN-PT PEMS exhibited a much lower, clinically relevant, 5 ng/ml concentration sensitivity, both obtained in a background of 1 mg/ml of bovine serum albumin (BSA) and with the same single-chain variable fragment (scFv) antibody, H3, immobilized on the same 3-mercaptopropyltrimethoxysilane (MPS) insulation surface.

More recent studies [17–19] showed that PEMS detection resonance frequency shift was primarily due to the elastic modulus change in the piezoelectric layer from the binding-induced surface stress. As a result, the mass sensitivity of a PMN-PT PEMS and that of a PZT PEMS were respectively 300 times [17,20] and 100 times [5–7,10,11,14] higher than could be accounted for by mass loading alone. With a DC bias electric field, the mass sensitivity of a PMN-PT PEMS was further enhanced to more than 1000 times higher than could be accounted for by mass loading alone [20]. These studies also revealed that PEMS exhibit high-frequency non-flexural resonance modes such as width and length extension modes [17,18] due to the presence of the highly piezoelectric layer that silicon-based microcantilevers lack. At the same time, it was also shown that as a result of the elastic modulus change mechanism, a PEMS relative resonance frequency shift, $\Delta f/f$, was directly proportional to the binding-induced surface stress and inversely proportional to the PEMS thickness [21] where f denotes a PEMS resonance frequency. This suggests that under the same detection conditions, Δf could be higher with a high-frequency resonance mode to result in higher detection sensitivity. As non-flexural extension mode resonance occur at a much higher frequency than flexural-mode resonance, detection using non-flexural resonance modes potentially can increase PEMS sensitivity without size reduction.

The purpose of this study is to investigate label-free, in situ detection of Her2 in diluted human serum using a PZT/glass PEMS about 1 mm in length with a 2 mm long glass tip with its *longitudinal extension mode*. A schematic of the first longitudinal-extension-mode vibration is shown in Fig. 1(b). For ease of comparison, the PZT PEMS will have a similar size to the previous PZT/glass PEMS, i.e., the PEMS was about 970 μm long and 580 μm wide consisting a 127 μm thick PZT layer bonded to a 75 μm thick glass of the same width with a glass tip about 1.8 mm long as shown in Fig. 2(a) about the same size as the PZT/glass PEMS used in earlier stud-

ies [10,11]. The PZT/glass PEMS will be insulated with the same MPS coating and the H3 scFv antibody will be immobilized on the MPS insulation surface [10,11]. We will explore using a longitudinal mode for Her2 detection and examine how using the longitudinal mode decreased the detection concentration limit. In addition, we will also explore using a PZT/glass PEMS as a tool to determine the Her2–H3 antigen–antibody dissociation constant, K_d. Because the detection concentration limit in the earlier Her2 detection studies using the flexural peaks of a PZT/glass PEMS was much higher than the preliminary BIAcore values of K_d, 3.4×10^{-8} M [11] it was not possible to reliably determine K_d using the earlier PZT/glass PEMS results. By using the longitudinal extension mode the detection concentration limit of a PZT/glass PEMS could be substantially lowered, it could then be possible to use PEMS as a tool to determine the H3–Her2 dissociation constant, K_d, from the detection results. We will also compare the K_d determined by the PEMS measurements with that measured by a BIAcore 1000 instrument (BIAcore, Piscataway, NJ).

Although high harmonics of flexural modes has been explored for better sensitivities in silicon-based microcantilevers [22] and in piezoelectric microcantilevers [8,10,11], the advantages of a longitudinal extension mode of a highly piezoelectric microcantilever over a higher flexural mode at the same frequency range are many. First, it has been shown that the height of a longitudinal extension resonance peak (in the phase angle of the electrical impedance versus frequency spectrum) of a PZT/glass PEMS similar to the PZT/glass PEMS used in this study was much greater than that of higher flexural resonance peaks at the same frequencies. This was a result of the large piezoelectric effect of the high piezoelectric layer. Because of strong resonance, traditionally, a longitudinal or width extension mode is used for piezoelectric coefficient determination [17,18]. This increase in peak height is important because it results in a higher quality factor. Alternative modes of vibration have been used in MEMS to increase the quality factor [23–26] because a higher quality factors allows for detection of smaller shifts in resonant frequency, which will increase the sensitivity of the sensor [27]. However, there has been no report on longitudinal modes of a silicon-based microcantilever presumably due to the difficulty in exciting and detecting such a mode. Furthermore comparison of the in-air and in-liquid resonance spectra of a PZT/glass PEMS showed the flexural peaks, especially the higher-frequency peaks diminished in liquid. In contrast, the first longitudinal peak exhibited little decrease in both the peak height and the peak frequency. That the longitudinal extension mode of a PZT/glass PEMS exhibited less damping effect than flexural modes was that the longitudinal extension vibration amplitude was much smaller than that of a flexural mode. For the above reasons, a longitudinal mode is more advantageous than a flexural mode for detection using a PEMS. It is of interest to note that the higher frequency peak of a PZT microcantilever used by Campbell and Mutharasan [28] was likely a longitudinal extension mode as well because their PZT microcantilever was made of the same PZT layer and the higher-frequency peak they used also exhibited a much higher peak height than other peaks as similar to that of the present work and that of McGovern et al. [7].

Finally the advantage of using a higher-frequency longitudinal mode of a PZT/glass PEMS instead of a flexural mode of a thinner PMN-PT PEMS [11] is that a PZT/glass PEMS is constructed from commercial PZT and cover glass, which is much easier than the PMN-PT PEMS where the PMN-PT freestanding films were fabricated in house from powder synthesis, to tape casting to sintering. The ability to use the longitudinal extension mode of a PZT/glass PEMS to achieve a higher sensitivity is of great interest because of the ease of fabrication as compared to PMN-PT PEMS or other micro-machined PZT PEMS [14,16].
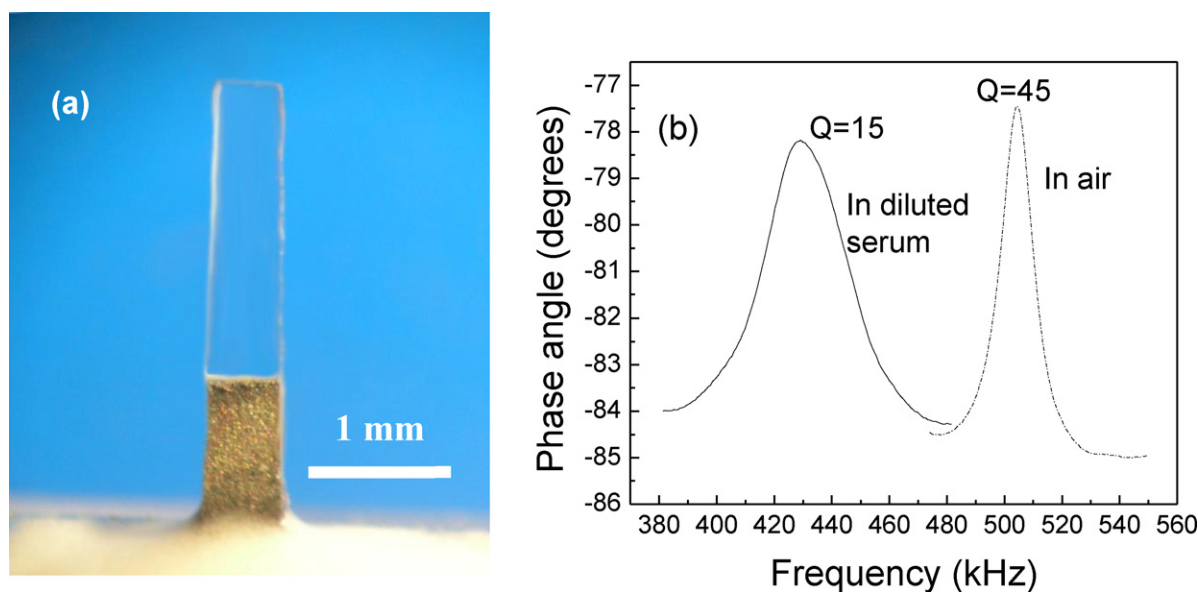
Fig. 2. (a) An optical micrograph and (b) in-air and in dilute serum resonance spectra of a 970 μm long and 580 μm wide PZT/glass PEMS with a 1800-μm long glass tip.

2. Experimental procedure

There were more than one PZT/glass PEMS used in this study. They were consisted of a commercial PZT layer (T105-H4E-602, Piezo System, Cambridge, MA) 127 μm thick, about 1000 μm long and 600 μm wide bonded to a 75 μm thick glass layer (Fisher Scientific, Pittsburgh, PA) with a glass tip about 1.8 mm long protruding from the free end. The PEMS was fabricated by first bonding the PZT layer to the glass layer using a nonconductive epoxy (Loctite, Rocky Hill, CT) and embedding the PZT/glass bilayer in wax. The PZT/glass assembly was then cut to strips with a wire saw (Princeton Scientific Precision, Princeton, NJ). After attaching the wires to the top and bottom electrodes using conductive glue (XCE 3104XL, Emerson and Cuming Company, Billerica, MA), a PZT/glass strip was glued to a glass substrate to form the microcantilever shape. Fig. 2(a) is an optical micrograph of the PZT/glass PEMS. The resonance peak used for this detection was the first longitudinal extension mode [29] at around 504 kHz in air with a Q value of 45 and around 429 kHz in diluted serum with a Q value of 15 as shown in the resonance spectra in Fig. 2(b). The decrease in the Q value was due to the viscous damping of the liquid while the decrease in the resonance frequency was the result of the mass of the surrounding liquid that moved in phase with the PEMS [30].

For the initial MPS deposition, the PEMS were first cleaned in a diluted (1:100 in water) piranha solution (two parts of 98% sulfuric acid (Fisher, Fair Lawn, NJ) with one part of 30% hydrogen peroxide (FisherBiotech, Fair Lawn, NJ)) at 20 °C for 1 min followed by soaking in a 40 mM MPS solution in ethanol covered with paraffin film for 4 h and rinsing by de-ionized (DI) water. They were then soaked in a 0.01 M NaOH solution overnight for cross-linking, followed by soaking in DI water for 1 h and overnight vacuum-oven drying (Model 1400E, VWR International) at 762 mm Hg to conclude the first MPS coating. For each of the subsequent MPS depositions, they were soaked overnight in a freshly prepared 40 mM MPS solution in ethanol titrated to pH 4.5 with acetic acid. This procedure was repeated two times to give a total of 3 MPS depositions to result in a MPS thickness of about 150 nm [10].

The target Her2 extracellular domain (ECD) was expressed from stably transfected HEK-293 cells and purified using immobilized metal affinity chromatography (IMAC) as previously described [31]. The anti-Her2 scFv, H3, was isolated from a naïve human scFv phage display library using techniques essentially as previously described [32]. Her2 ECD obtained as described above was coated onto a Maxisorp-Immunotube (NUNC, Denmark) at a concentration of 20 μg/ml in coating buffer (Bup-H carbonate bicarbonate buffer; Pierce) at 4 °C, overnight. scFv-Phage library stock (100 μl; 1.3×10^{13} pfu/ml) was added to the immunotubes to pan (isolate) anti-Her2 scFv-phage clones. The H3 clone was isolated following four rounds of selection, was sequenced and subcloned into the pCyn expression vector. Soluble scFv were expressed in *Escherichia coli* TG1, isolated from the periplasmic space and purified by Ni-NTA agarose affinity chromatography and HPLC on a Superdex75 column (Pharmacia) as previously described [33]. Final yields were 1–2 mg of pure H3 scFv per liter of expression culture. Specificity for Her2 ECD was confirmed by surface plasmon resonance on a BIAcore 1000 instrument and by flow cytometry against Her2 overexpressing human tumor cell lines.Sulfosuccinimidyl-4-(*N*-maleimidomethyl)cyclohexane-1-carboxylate (sulfo-SMCC) (Pierce) was used as the bi-functional linker for scFv immobilization on MPS. First, the scFv was linked to sulfo-SMCC using a 1 ml solution 900 nM scFv and 80 μM sulfo-SMCC for 2 h at 4 °C. The NHS-ester in the sulfo-SMCC will react with a primary amine of the scFv. Unreacted sulfo-SMCC molecules were then removed by repeating microcentrifugation at 6000 RPM with a 10 kD filter (Millipore) three times. The MPS-coated PEMS was then soaked in the sulfo-SMCC-linked scFv solution with 5 mM ethylenediaminetetraacetic acid (EDTA) (Pierce) for 2 h to immobilize the scFv on the MPS coating surface via the reaction of the maleimide of the sulfo-SMCC with the sulfhydryl of the MPS. In a previous study we have verified this immobilization on multiple PEMS platforms [10]. The adsorption density, Γ, of the SMCC-linked scFv on the MPS was estimated to be $\Gamma = 7$ ng/mm² from a separate measurement using a quartz crystal microbalance [10].

It is important to minimize nonspecific binding so that even weak signals at low Her2 concentrations can be clearly distinguished. It is therefore essential, following coating of the PEMS with scFv, to saturate the remaining surface that is not covered with scFv with molecules that are abundant in serum such as serum albumin, human IgG, or substances similar to serum such as fetal calf serum (FCS), bovine serum albumin (BSA), and normal human, goat or horse sera at concentrations ranging between 1% and 10% [34]. After such saturation procedure, Tween 20, a surfactant, is often added to the washing buffer because it has also been shown to reduce nonspecific binding. As human serum typically contains
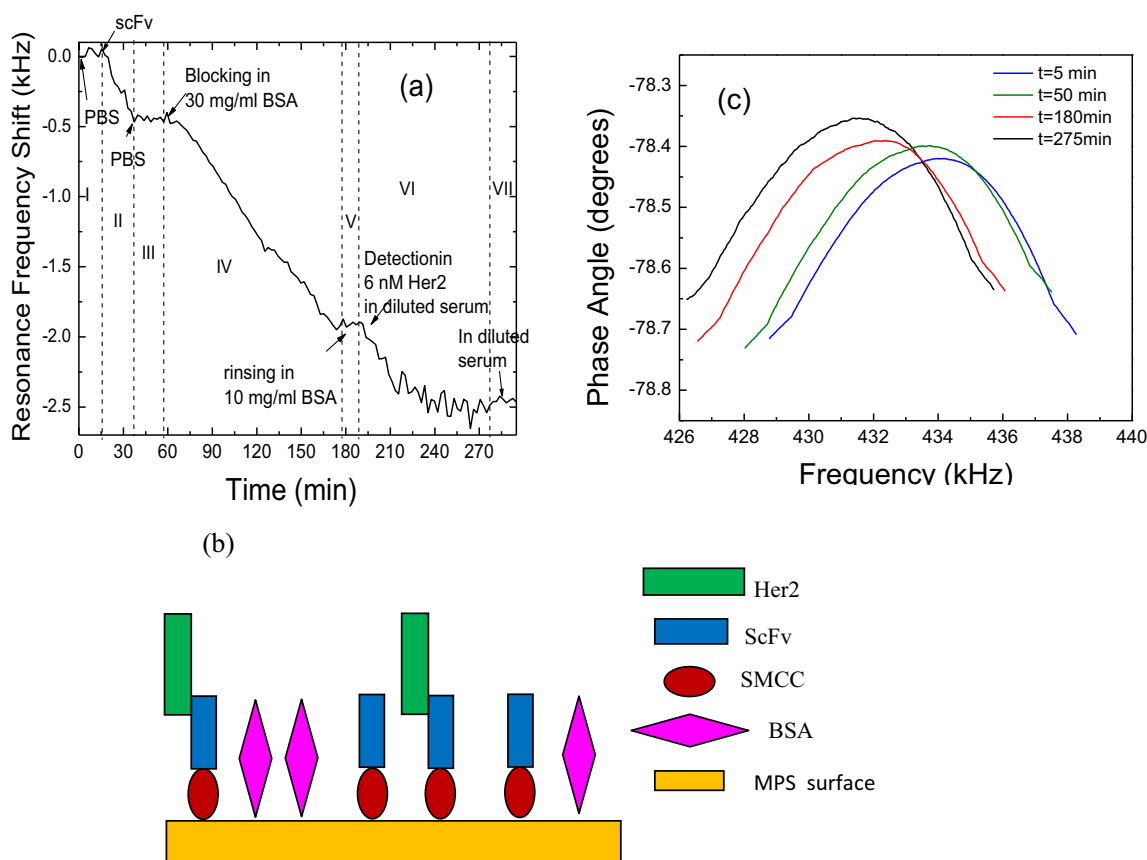
Fig. 3. (a) Resonance frequency shift versus time of the PEMS: in PBS in period I at $t = 0$–15 min, scFv immobilization in period II at 15–44 min, PBS rinsing in period III at 43–59 min, 30 mg/ml BSA blocking in period IV at 59–185 min, 10 mg/ml BSA rinsing and Tween20 rinsing in period V, detection in 6 nM Her2 in 1 in 40 diluted serum in period VI at $t = 185$–278 min and rinsing in diluted serum in period VII at $t = 278$–300 min, (b) a schematic showing the immobilized scFv on the MPS surface, BSA covering the MPS surface not occupied by the scFv, and Her2 binding to the scFv on the MPS surface, and (c) phase angle versus frequency resonance spectra at $t = 5$ min (in PBS), 50 min (after scFv immobilization), 180 min (after BSA blocking), and 275 min (after Her2 detection). Note that throughout the detection period, the shape of the resonance peak and the Q value remained constant.

about 40 mg/ml of albumin which helps maintain the blood osmotic pressure to prevent leaking of the fluid from the blood to tissues. Serum albumin is by far the most abundant protein in serum and the major source of potential non-specific binding. To minimize potential non-specific binding in diluted serum (1) we carried out the detection in 1 in 40 diluted human serum (one part of human serum with 40 parts of PBS, and (2) blocked the sensor surface with a 30 mg/ml BSA (bovine serum albumin) solution in PBS followed by rinsing with a solution containing 10 mg/ml BSA and 0.1% Tween20 in PBS prior to detection.

For Her2 detection, the scFv-immobilized PEMS was then immersed in a home-built flow cell [7,8] with a peristaltic pump (model 77120-62, Cole-Parmer's Master Flex, Vernon Hills, IL) for both BSA blocking and Her2 detection with the PEMS's two faces tangential to the flow at a flow rate of 0.7 ml/min. The flow cell contained 6 ml of liquid.

3. Results

3.1. In situ all-electrical detection of Her2 in diluted serum

To illustrate the real-time nature of the PEMS, after the scFv was chemically bonded to SMCC as described above, a MPS-coated PEMS was then placed in the flow cell and subjected to scFv immobilization, BSA blocking, and Her2 detection at a flow rate of 0.7 ml/min. The resonance frequency shift versus time in this sequence is shown in Fig. 3(a). It started with immersing the PEMS in PBS for 15 min in period I at $t = 0$–15 min. Note that during this

period, Δf remained stable with no observable down shifting. The PBS period was followed with the immobilization of the SMCC-linked scFv in period II at $t = 15$–44 min in which the resonance frequency of PEMS decreased with time, yielding a resonance frequency down shift of roughly −430 Hz at = 44 min. After the scFv immobilization procedure, PBS was then flown for 15 min in period III at $t = 44$–59 min to remove any unbound scFv from the flow cell. During this second PBS period, the resonance frequency of PEMS was stable with no observable down shifting. Between $t = 59$ min to 185 min in period IV, a 30 mg/ml BSA solution in PBS was flown in the flow cell to preemptively saturate the unoccupied sites on the sensor surface with BSA to minimize potential non-specific binding later in the Her2 detection in diluted human serum. A schematic illustrating scFv immobilized on the MPS surface, BSA covering the MPS surface not occupied by the scFv, and Her2 binding to the scFv on the MPS surface is shown in Fig. 3(b). Note that the resonance frequency down shift due to the non-specific BSA binding to the unoccupied sites saturated at around $t = 172$ min, yielding a net resonance frequency shift of about −1470 Hz. Following the BSA blocking, the PEMS was rinsed with a 10 mg/ml BSA and 0.1% Tween20 solution in period V at $t = 185$–195 min. Again, during this rinsing period, the resonance frequency of the PEMS remained fairly stable throughout. The PEMS was then exposed to the flow of diluted human serum containing 600 ng/ml of Her2 in period VI at $t = 185$–278 min over which time period the PEMS exhibited a resonance frequency shift of −520 Hz. A final background check of flow of diluted serum was conducted in period VII at $t = 278$–295 min. As can be seen, in period VII, the resonance

frequency of the PEMS also remained stable in diluted serum after the detection. The adsorption density, Γ, scFv on the MPS was estimated to be $\Gamma = 7\,ng/mm^2$ from a separate measurement using a quartz crystal microbalance [10]. Given that the PEMS had Δf about $-0.44\,kHz$ for scFv immobilization, about $-1.47\,kHz$ for BSA blocking, and $0.65\,kHz$ for Her2 detection at 6 nM, it follows that the amount of BSA bound on the PEMS surface was $(7\,ng/mm^2)((-1.47\,kHz)/(-0.44\,kHz)) = 23\,ng/mm^2$, and that of Her2 at 6 nM was $(7\,ng/mm^2)((-0.65\,kHz)/(-0.44\,kHz)) = 10\,ng/mm^2$ provided that the amount of protein bound on the sensor surface was proportional to the sensor's resonance frequency shift.

To demonstrate that the resonance frequency shifts shown in Fig. 3(a) at various times were indeed reliable, we show the phase angle versus frequency resonance spectra of the PEMS at $t = 5\,min$ in PBS, at $t = 50\,min$ after the scFv immobilization, at $t = 180\,min$ after the BSA blocking, and at $t = 275\,min$ after the Her2 detection during the above test in Fig. 3(c). Note this PEMS was only used for illustrating the blocking and detection procedure and was different from the PEMS shown in Fig. 2. As can be seen, the shape and height of the resonance peak remained roughly constant throughout the test, indicating that the resonance frequency shifts shown in Fig. 3(a) were indeed reliable. These results were similar to our previous work on Her2 detection in mixed protein solutions using a flexural mode resonance peak of a PZT/glass PEMS except that with the present longitudinal extension resonance peak the PEMS was able to detect Her2 at a concentration of 600 ng/ml which was much lower than the μg/ml concentration limit of a PZT/glass PEMS when flexural-mode resonance peaks were used [10,11].

3.2. Her2 dose response in 1 in 40 diluted human serum

To find out the detection concentration limit of the longitudinal extension mode of a PZT/glass PEMS, we examine the dose response of Her2 in diluted human serum using the PEMS shown in Fig. 2(a) and (b). Before each detection experiment, the PEMS was stripped of the bound scFv and reinsulated with MPS. Fresh scFv was then immobilized on the PEMS surface using procedures described in Section 2. The PEMS was then subject to a PBS flow across the PEMS surface for 10 min to establish the background followed by 30 mg/ml BSA blocking in a flow until the resonance frequency of the PEMS saturated (about 2 h) followed by rinsing with 10 mg/ml BSA and 0.1% Tween 20. The PEMS was then exposed to diluted human serum spiked with Her2 in one of the following concentrations: 60,000, 6000, 600, 60, and 6 ng/ml. In this study, we re-immobilize the scFv after each detection as opposed to simply releasing the Her2 in a glycine/HCl buffer solution [5,6,10,11,35] after detection to ensure that the binding performance of the scFv in each detection was roughly identical. The obtained resonance frequency shift versus time in diluted serum with 60,000, 6000, 600, 60, 6, and 0 ng/ml (corresponding to 600, 60, 6, 0.6, 0.06, and 0 nM) of Her2 is shown in Fig. 4(a) where each curve was the average of three independent tests. The curves presented in Fig. 4 were produced by averaging the sensor response over 3 trials, and the standard deviation between trials is depicted using the error bars. The Δf measured were -2200 ± 120, -1082 ± 180, -528 ± 57, -194 ± 70, and $-28 \pm 40\,Hz$ for 60,000, 6000, 600, 60, and 6 ng/ml of Her2 in diluted serum, respectively. To better illustrate the Δf versus time at low concentrations, we show the Δf versus time at 0, 0.06, and 0.6 nM in Fig. 4(b). Note that at 0 ng/ml of Her2 in diluted serum (the control), the PEMS exhibited a time averaged Δf of 1 Hz and a standard deviation of 4 Hz over 60 min, indicating the PEMS was stable in diluted serum. At Her2 concentrations from 6 to 60,000 ng/ml, the magnitude of the resonance frequency shift initially increased with time and saturated more or less after $t = 50\,min$. Therefore, the time average of the resonance frequency shifts over the period $t = 50$–60 min at each concentra-
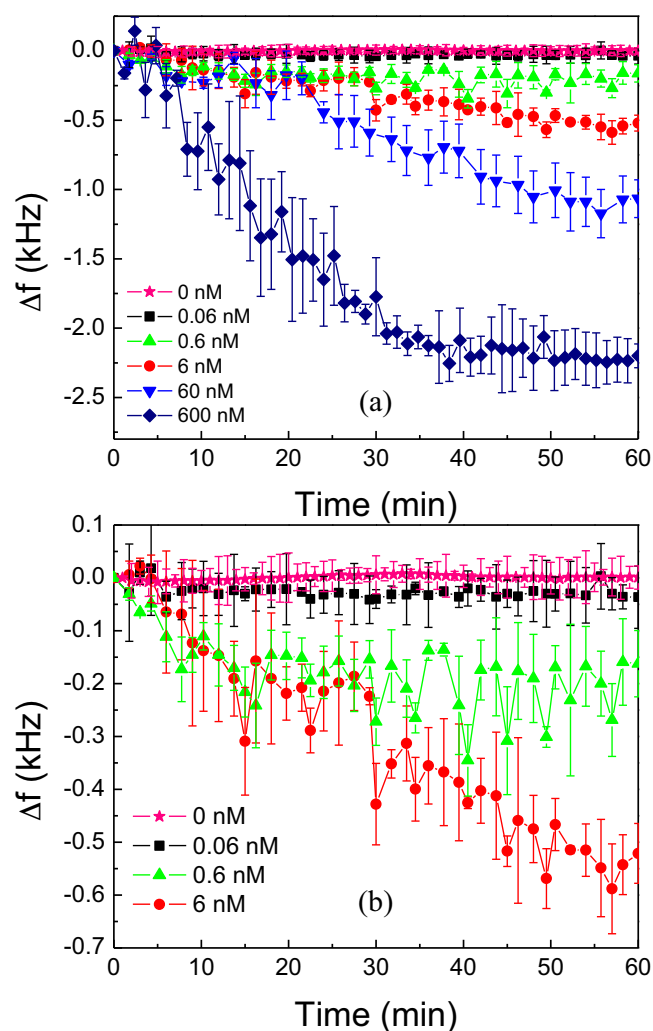

Fig. 4. (a) Resonance frequency shift, Δf, versus time of the PEMS in diluted serum spiked with 0 nM (stars), 0.06 nM (squares), 0.6 nM (up triangles), 6 nM (circles), 60 nM (down triangles), and 600 nM (diamonds) of Her2. The curve presented is the average sensor response of 3 trials, and the standard deviation between trials is depicted using the error bars. The Δf measured were -2200 ± 120, -1082 ± 180, -528 ± 57, -194 ± 70, and $-28 \pm 40\,Hz$ for 60,000, 6000, 600, 60, and 6 ng/ml of Her2 in diluted serum, respectively. (b) The blowup of Δf versus time at low concentrations.

tion was obtained to approximate the "equilibrium" resonance frequency shifts, Δf. This method for calculating Δf was described in a previous publication [36]. The obtained Δf were -2200 ± 53, -1082 ± 54, -528 ± 38, -194 ± 42, and $-28 \pm 15\,Hz$ for 60,000, 6000, 600, 60, and 6 ng/ml of Her2 in diluted serum, respectively. Note that the standard deviation for the "equilibrium" Δf obtained above was essentially the half bandwidth of Δf at $t = 50$–60 min. Using this definition, the "equilibrium" Δf at $t = 60\,min$ for 0 ng/ml Her2 concentration was approximately $1 \pm 1\,Hz$. The smaller standard deviation (1 Hz) obtained over $t = 50$–60 min than the 4 Hz standard deviation over the entire 60 min was presumably due to the smaller time interval of only 10 min. Clearly, the obtained "equilibrium" Δf of $28 \pm 15\,Hz$ shift at $t = 60\,min$ at 6 ng/ml (0.06 nM) was well above the 4 Hz standard deviation of the control over 60 min (or 1 Hz over the last 10 min), indicating the validity of the obtained Δf at this concentration. The reason for the slow, almost linear response over the 60 min of detection at this concentration was in part due to the low concentration as well as the moderately low affinity of this scFv. It is also worth noting that the fluctuations of Δf with time were higher at a higher Her2 con-
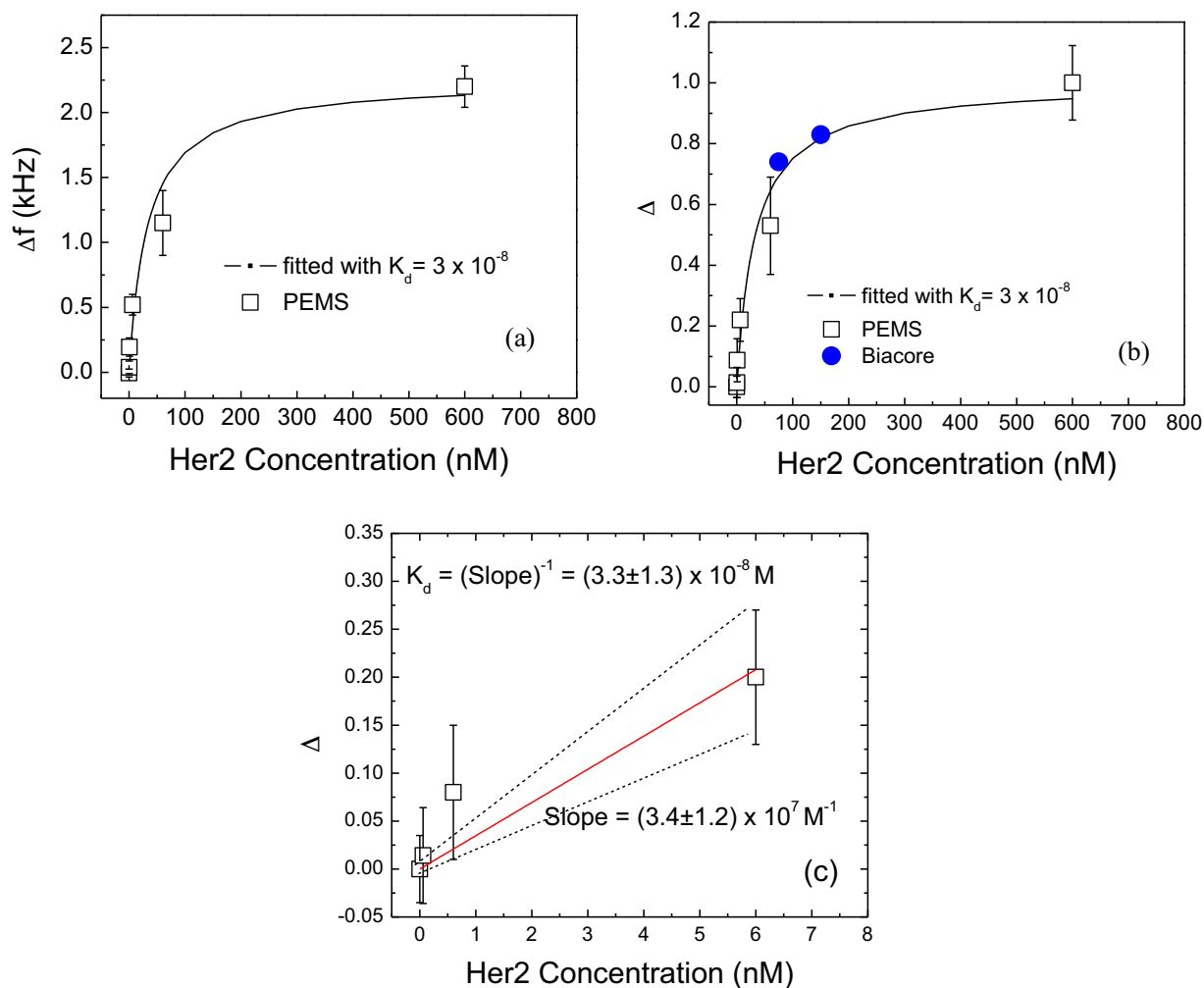
Fig. 5. (a) Resonance frequency shift, Δf, at $t = 60$ min versus c and (b) θ versus c where c was the Her2 concentration, $\theta = \Delta f / \Delta f_s$ with $\Delta f_s = -2250$ Hz approximated as the Δf at $t = 60$ min at 600 nM. The solid line in (a) and (b) were calculated Δf and θ based on $K_d = 3 \pm 0.3 \times 10^{-8}$ M, respectively. Also plotted in (b) are the results from BIAcore (full circles), which was in agreement with the PEMS results.

centration. Even at the late stage of the detection at $t = 50$–60 min where the binding of Her2 almost saturated the standard deviations over this period were still 53, 54, 38, 42 Hz at 60,000, 6000, 600, 60 ng/ml of Her2, respectively higher than the 15 Hz at 6 ng/ml and the 4 Hz standard deviation over 60 min or the 1 Hz standard deviation at $t = 50$–60 min at 0 ng/ml of Her2. The same trend of larger Δf fluctuations with time at a higher concentration has also been observed in in situ detection of other biological systems [5–7,10,11,13]. It was likely that the fluctuations of Δf during detection were related to binding, unbinding and re-arrangement of the antigen on the sensor surface. Such binding, unbinding events have been in situ illustrated by the binding and unbinding events of single *Cryptosporidium parvum* oocysts in CP detection at extreme low concentrations (1 Cp/10 ml) [7].

3.3. Determination of the dissociation constant, K_d using PEMS

In Fig. 5(a), we plot Δf versus Her2 concentration, c where Δf was the equilibrium resonance frequency shift approximated by the time averaged resonance frequency shift in the period $t = 50$–60 min. The data points in Fig. 5(a) and (b) are the average of 2–3 independent runs with error bars indicating the variation in sensor response between trials. Because the preliminary K_d obtained by earlier BIAcore studies was 3.4×10^{-8} M, which was about 18 times smaller than the concentration of 600 nM

at 60,000 ng/ml, we thus approximated the Δf at 60,000 ng/ml, -2200 Hz as the equilibrium saturated resonance frequency shift, Δf_s. The fraction of saturation, θ, which is defined as the equilibrium fraction of bound binding sites out of all available binding sites on the sensor surface can be estimated as the ratio of the equilibrium resonance frequency shift $\Delta f(c)$ at concentration c to Δf_s. Approximating the Δf at concentration c as the equilibrium $\Delta f(c)$, the equilibrium fraction of saturation can then be deduced as $\theta = \Delta f(c)/\Delta f_s$. The obtained θ versus c is plotted as open squares in Fig. 5(b). The equilibrium dissociation constant, K_d is related to the Her2 concentration, c, as

$$\theta = \frac{c/K_d}{1 + c/K_d}. \tag{1}$$

With Eq. (1), the best fit to the data points in Fig. 5(b) could be obtained with $K_d = 3.3 \pm 0.3 \times 10^{-8}$ M. The solid line in Fig. 5(b) was obtained with $K_d = 3.3 \times 10^{-8}$ M. As can be seen, the solid line agreed well with the experimental data points, indicating the deduced K_d was reasonable.

Using the theoretical curve, an estimation of K_d was obtained based on the data points with $\theta < 0.2$ as an independent check of the fit shown in Fig. 5(a) and (b). Note that with Eq. (1) where c is the Her2 concentration and K_d the dissociation constant, θ can be approximated as $\theta \cong c/K_d$ for $c/K_d \leq 0.2$ (or $\theta < 0.2$). This indicates that if θ versus c is plotted in the range of
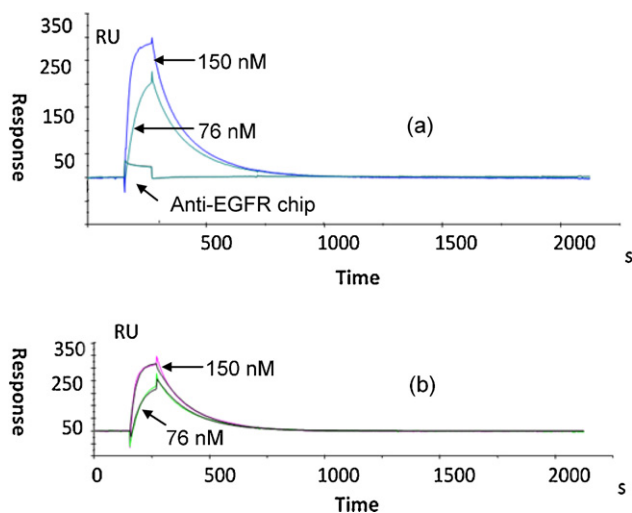
Fig. 6. (a) BIAcore response versus time of the H3-coated chips and anti-EGFR-coated control chips at 150 and 76 nM and (b) the BIAcore response of the H3-coated chips versus time after subtracting the response of anti-EGFR-coated control chips.

$\theta < 0.2$, the inverse of the slope would approximate K_d. Such a separate analysis in the range of $\theta < 0.2$ would provide an independent check for the fit for the entire concentration range using $K_d = 3 \times 10^{-8}$ M. In Fig. 5(c), we plot θ versus c for $\theta < 0.2$. The slope of Fig. 5(c) is $(3.4 \pm 1.2) \times 10^7$ M^{-1}. The inverse of this slope yielded $K_d = (3.3 \pm 1.3) \times 10^{-8}$ M, consistent with the value 3×10^{-8} M used to generate the solid lines in Fig. 5(a) and (b), indicating that the fit shown in Fig. 5(a) and (b) is reasonable.

3.4. K_d validation by BIAcore measurements

The binding kinetics of H3 scFv to Her2 was also examined using a BIAcore 1000 instrument (BIAcore, Piscataway, NJ) using recombinant Her2 bound to a CM5 sensor chip with epidermal growth factor receptor (EGFR) bound to a different CM5 sensor chip as the reference. The response of the BIAcore was recorded at H3 scFv concentrations 150 nM and 76 nM across the Her2 and EGFR chips, and the results are shown in Fig. 6(a). The response measured from the EGFR chip was used as an assessment of the background and was subtracted from the response measured for the Her2 chip. The response of the Her2 chip after the background correction is shown in Fig. 6(b). Sections of the curve associated with H3 binding and unbinding were then fitted to the following equation:

$$\frac{dR}{dt} = k_a c(R_{max} - R) - k_d R, \tag{2}$$

where R and R_{max} were the response signal and the maximum response signal at saturation, respectively, t the time, c the H3 concentration, and k_a and k_d were the association and dissociation rate constants, respectively. The value for k_a was deduced to be 2.3×10^5 M^{-1} s^{-1} and k_d to be 6.8×10^{-3} s^{-1}. Using these values, the equilibrium dissociation constant $K_d = k_d/k_a$ was deduced to be 3×10^{-8} M. Combining with the result of 3.4×10^{-8} M that we obtained earlier, we had a K_d of $3.2 \pm 0.3 \times 10^{-8}$ in agreement with the $3.3 \pm 0.3 \times 10^{-8}$ M obtained by the PEMS.

In addition to obtaining K_d from k_a and k_d as deduced from the adsorption and desorption sections of the BIAcore curves, the fractional equilibrium response, θ, used in Eq. (1) could also be obtained as the ratio of the equilibrium response, R, to the maximum response R_{max}, as R/R_{max}. With $R_{max} = 308$ RU, the values of θ were determined to be 0.83 and 0.74 for 150 nM and 76 nM, respectively. These values were also plotted in Fig. 5(b) as full circles. Clearly, the full circles from the BIAcore measurements

fell on the solid line deduced by the PEMS results, indicating the agreement of the K_d value determined from BIAcore based on the fractional equilibrium response with the results obtained with the PEMS. The deduced K_d value from the BIAcore data by fitting to Eq. (1) was also 3×10^{-8} M, again, in agreement with the PEMS result of $3.3 \pm 0.3 \times 10^{-8}$ M. In addition, the χ^2 parameter [37] of the present BIAcore measurements was 6, smaller than 10, indicative that the values for k_a, k_d, K_d deduced from the BIAcore were statistically valid [37], further confirming the validity of the K_d value determined by the PEMS. In a recent study, Lin et al. measured K_d using a dual-polarization interferometric (DPI) biosensor and compared with that obtained by ELISA [38]. They showed that the K_d obtained by the DPI method was in close agreement with that obtained by ELISA, indicating that carefully measured K_d values could be independent of the methods used and supporting our comparison of the K_d obtained by the PEMS with that obtained by the BIAcore.

4. Conclusion

We have investigated real-time, label-free, in situ detection of Her2 in diluted serum using the first longitudinal extension mode of a PZT/glass PEMS with H3 scFv immobilized on the MPS insulation layer of the PEMS surface. We showed that with the longitudinal extension mode, a PZT/glass PEMS consisting of a 1 mm long and 127 mm thick PZT layer bonded with a 75 mm thick glass layer with a 1.8 mm long glass tip could detect Her2 at a concentration of 6–60 ng/ml (or 0.06–0.6 nM) in diluted human serum, which were about 100 times lower than the concentration limit using the lower-frequency flexural mode of a PZT/glass PEMS of similar dimensions. With such concentration sensitivity, we further showed that PEMS could be used to accurately determine the equilibrium H3–Her2 dissociation constant K_d. The $K_d = 3.3 \pm 0.3 \times 10^{-8}$ M as deduced by the PEMS measurements. The value for K_d deduced by BIAcore was also $3.2 \pm 0.3 \times 10^{-8}$ M, consistent with that obtained by PEMS.

Acknowledgments

References

[1] F.J. Esteva, C.D. Cheli, H. Fritsche, M. Fornier, D. Slamon, R.P. Thiel, D. Luftner, F. Ghani, Clinical utility of serum HER2/neu in monitoring and prediction of progression-free survival in metastatic breast cancer patients treated with trastuzumab-based therapies, Breast Cancer Res. 7 (2005) R436–R443.

[2] R. Dittadi, M. Zancan, A. Perasole, M. Gion, Evaluation of HER-2/neu in serum and tissue of primary and metastatic breast cancer patients using an automated enzyme immunoassay, Int. J. Biol. Markers 16 (2001) 255–261.

[3] T. Fehm, G. Gebauer, W. Jager, Clinical utility of serial serum c-erbB-2 determinations in the follow-up of breast cancer patients, Breast Cancer Res. Treat. 75 (2002) 97–106.

[4] A. Meenakshi, R.S. Kumar, N.S. Kumar, ELISA for quantitation of serum C-erbB-2 oncoprotein in breast cancer patients, J. Immunoassay Immunochem. 23 (2002) 293–305.

[5] Q. Zhu, W.Y. Shih, W.H. Shih, Real-time, label-free, all-electrical detection of Salmonella typhimurium using lead titanate zirconate/gold-coated glass cantilevers at any relative humidity, Sens. Actuators B: Chem. 125 (2007) 379–388.

[6] Q. Zhu, W.Y. Shih, W.H. Shih, In situ, in-liquid, all-electrical detection of Salmonella typhimurium using lead titanate zirconate/gold-coated glass cantilevers at any dipping depth, Biosens. Bioelectron. 22 (2007) 3132–3138.

[7] J.-P. McGovern, W.Y. Shih, R. Rest, M. Purohit, Y. Pandya, W.-H. Shih, Label-free flow-enhanced specific detection of *Bacillus anthracis* using a piezoelectric microcantilever sensor, Analyst 133 (2008) 649–654.

[8] J.-P. McGovern, W.Y. Shih, W.-H. Shih, In situ detection of *Bacillus anthracis* spores using fully submersible, self-exciting, self-sensing PMN-PT/Sn piezoelectric microcantilevers, Analyst 132 (2007) 777–783.

[9] J.A. Capobianco, W.Y. Shih, W.-H. Shih, Methyltrimethoxysilane-insulated piezoelectric microcantilevers for direct, all-electrical biodetection in buffered aqueous solutions, Rev. Sci. Instrum. 77 (2006) 125105.

[10] J.A. Capobianco, W.Y. Shih, W.-H. Shih, 3-Mercaptopropyltrimethoxysilane as insulating coating and surface for protein immobilization for piezoelectric microcantilever sensors, Rev. Sci. Instrum. 78 (2007) 046106.

[11] J.A. Capobianco, W.Y. Shih, Q.-A. Yuan, G.P. Adams, W.-H. Shih, Label-free all-electrical, in situ human epidermal growth receptor 2 detection, Rev. Sci. Instrum. 79 (2008) 076101.

[12] J.W. Yi, W.Y. Shih, R. Mutharasan, W.H. Shih, In situ cell detection using piezoelectric lead zirconate titanate-stainless steel cantilevers, J. Appl. Phys. 93 (2003) 619–625.

[13] J.W. Yi, W.Y. Shih, W.H. Shih, Effect of length, width, and mode on the mass detection sensitivity of piezoelectric unimorph cantilevers, J. Appl. Phys. 91 (2002) 1680–1686.

[14] J.H. Lee, K.S. Hwang, J. Park, K.H. Yoon, D.S. Yoon, T.S. Kim, Immunoassay of prostate-specific antigen (PSA) using resonant frequency shift of piezoelectric nanomechanical microcantilever, Biosens. Bioelectron. 20 (2005) 2157–2162.

[15] Z. Shen, W.Y. Shih, W.-H. Shih, Mass detection sensitivity of piezoelectric cantilevers with a nonpiezoelectric extension, Rev. Sci. Instrum. 77 (2006) 065101–065110.

[16] Z. Shen, W.Y. Shih, W.-H. Shih, Self-exciting, self-sensing PbZr$_{0.53}$Ti$_{0.47}$O$_3$/SiO$_2$ piezoelectric microcantilevers with femtogram/Hertz sensitivity, Appl. Phys. Lett. 89 (2006) 023506–023506-03.

[17] Q. Zhu, W.Y. Shih, W.-H. Shih, Mechanism of flexural resonance frequency shift of a piezoelectric microcantilever sensor during humidity detection, Appl. Phys. Lett. 92 (2008) 183505–183505-03.

[18] Q. Zhu, W.Y. Shih, W.-H. Shih, Mechanism of the flexural resonance frequency shift of a piezoelectric microcantilever sensor in a dc bias electric field, Appl. Phys. Lett. 92 (2008) 033503–033503-03.

[19] W.Y. Shih, Q. Zhu, W.-H. Shih, Length and thickness dependence of longitudinal flexural resonance frequency shifts of a piezoelectric microcantilever sensor due to Young's modulus change, J. Appl. Phys. 104 (2008) 074503–074505.

[20] Q. Zhu, W.Y. Shih, W.H. Shih, Enhanced detection resonance frequency shift of a piezoelectric microcantilever sensor by a DC bias electric field in humidity detection, Sens. Actuators B: Chem. 138 (2009) 1–4.

[21] J.A. Capobianco, Piezoelectric microcantilever serum protein detector, in: Materials Science and Engineering, Drexel University, Philadelphia, 2009, p. 272.

[22] T. Braun, M.K. Ghatkesar, N. Backmann, W. Grange, P. Boulanger, L. Letellier, H.-P. Lang, A. Bietsch, C. Gerber, M. Hegner, Quantitative time-resolved measurement of membrane protein–ligand interactions using microcantilever array sensors, Nat Nano 4 (2009) 179–185.

[23] L.A. Beardslee, K.S. Demirci, Y. Luzinova, B. Mizaikoff, S.M. Heinrich, F. Josse, O. Brand, Liquid-phase chemical sensing using lateral mode resonant cantilevers, Anal. Chem. 82 (2010) 7542–7549.

[24] Y. Liu, X. Li, Z. Zhang, G. Zuo, Z. Cheng, H. Yu, Nanogram per milliliter-level immunologic detection of alpha-fetoprotein with integrated rotating-resonance microcantilevers for early-stage diagnosis of heptocellular carcinoma, Biomed. Microdevices 11 (2009) 183–191.

[25] G. Piazza, P. Stephanou, A. Pisano, Piezoelectric aluminum nitride vibrating contour-mode MEMS resonators, J. Microelectrochem. Syst. 15 (2006) 1406–1418.

[26] W. Xu, S. Choi, J. Chae, A contour-mode film bulk acoustic resonator of high quality factor in a liquid environment for biosensing applications, Appl. Phys. Lett. 96 (2010), 053703–053703-03.

[27] H. Zhang, et al., A film bulk acoustic resonator in liquid environments, J. Micromech. Microeng. 15 (2005) 1911.

[28] G.A. Campbell, R. Mutharasan, Method of measuring *Bacillus anthracis* spores in the presence of copious amounts of *Bacillus thuringiensis* and *Bacillus cereus*, Anal. Chem. 79 (2007) 1145–1152.

[29] J.A. Capobianco, W.-H. Shih, J.-H. Leu, G.C.-F. Lo, W.Y. Shih, Label free detection of white spot syndrome virus using lead magnesium niobate-lead titanate piezoelectric microcantilever sensors, Biosens. Bioelectron. 26 (2010) 964–969.

[30] W.Y. Shih, X. Li, H. Gu, W.-H. Shih, I.A. Aksay, Simultaneous liquid viscosity and density determination with piezoelectric unimorph cantilevers, J. Appl. Phys. 89 (2001) 1497–1505.

[31] E. Horak, T. Heitner, M.K. Robinson, H.H. Simmons, J. Garrison, M. Russeva, P. Furmanova, J. Lou, Y. Zhou, Q.A. Yuan, L.M. Weiner, G.P. Adams, J.D. Marks, Isolation of scFvs to in vitro produced extracellular domains of EGFR family members, Cancer Biother. Radiopharm. 20 (2005) 603–613.

[32] Q.A. Yuan, H.H. Simmons, M.K. Robinson, M. Russeva, W.A. Marasco, G.P. Adams, Development of engineered antibodies specific for the Mullerian inhibiting substance type II receptor: a promising candidate for targeted therapy of ovarian cancer, Mol. Cancer Ther. 5 (2006) 2096–2105.

[33] G.P. Adams, R. Schier, K. Marshall, E.J. Wolf, A.M. McCall, J.D. Marks, L.M. Weiner, Increased affinity leads to improved selective tumor delivery of single-chain Fv antibodies, Cancer Res. 58 (1998) 485–490.

[34] M. Steinitz, Quantitation of the blocking effect of Tween 20 and bovine serum albumin in ELISA microwells, Anal. Biochem. 282 (2000) 232–238.

[35] C. Grogan, R. Raiteri, G.M. O'Connor, T.J. Glynn, V. Cunningham, M. Kane, M. Charlton, D. Leech, Characterisation of an antibody coated microcantilever as a potential immuno-based biosensor, Biosens. Bioelectron. 17 (2002) 201–207.

[36] L. Loo, J.A. Capobianco, W. Wu, X. Gao, W.Y. Shih, W.H. Shih, K. Pourrezaei, M.K. Robinson, G.P. Adams, Highly sensitive detection of HER2 extracellular domain in the serum of breast cancer patients by piezoelectric microcantilevers, Anal. Chem. 83 (2011) 3392–3397.

[37] G. De Crescenzo, S. Grothe, R. Lortie, M.T. Debanne, M. O'Connor-McCourt, Real-time kinetic studies on the interaction of transforming growth factor alpha with the epidermal growth factor receptor extracellular domain reveal a conformational change model, Biochemistry 39 (2000) 9466–9476.

[38] S. Lin, C.-K. Lee, Y.-H. Lin, S.-Y. Lee, B.-C. Sheu, J.-C. Tsai, S.-M. Hsue, Homopolyvalent antibody–antigen interaction kinetic studies with use of a dualpolarization interferometric biosensor, Biosens. Bioelectron. 22 (2006) 715–721.

Biographies

Joseph Capobianco is a multidisciplinary scientist, and entrepreneur with progressive experience in the development of sensors, and electronic materials. In 2004 he received a B.S. degree from the School of Biomedical Engineering and Health Systems at Drexel University, and subsequently completed a PhD in Materials Science and Engineering at Drexel University in 2009. His research has spanned multiple disciplines with research topics involving biological and chemical sensors, surface, organometallic, and colloidal chemistry, electronic ceramics and biological polymers. He is currently a senior scientist at ESL ElectroScience, where he develops electronic materials (conductors, insulators, semiconductors, and dielectrics) which are used for hybrid circuits, multilayer microelectronics, high and low temperature co-fired ceramics (HTCC&LTCC), metal to ceramic seals, solid oxide fuel cells, and organic light emitting diode (OLED) displays.

Wan Y Shih is an associate professor in the School of Biomedical Engineering, Science, and Health Systems at Drexel University. She received her BS in physics in 1976 from Tsing-Hua University in Taiwan and her PhD in Physics in 1984 from Ohio State University. She was a Research Scientist in the Department of Materials Science and Engineering at University of Washington in 1985–1993. She became a Research Scientist in the Princeton Institute of Materials at Princeton University in 1993–2000 and a Research Associate Professor in the Department of Materials Science and Engineering at Drexel University in 1993–2006. She joined School of Biomedical Engineering, Science, and Health Systems at Drexel University in 2006. Her research has covered a wide range of areas such as superconductivity, colloidal ceramics, piezoelectric materials and devices, and semiconducting nanoparticles. Her recent focus is on the biomedical applications of piezoelectric devices and photoluminescent semiconducting nanoparticles. She received the American Ceramic Society 1999 Edward C. Henry Electronics Division Best Paper Award for her work in the fundamental understanding of piezoelectric unimorph cantilevers and disks.

Gregory Adams is an Associate Professor and the Co-Leader, Developmental Therapeutics Program at the Fox Chase Cancer Center (FCCC) in Philadelphia, PA. He received a B.A. from the University of California, Santa Cruz in 1983 and a Ph.D. in Immunology from the University of California at Davis in 1991. He performed his postdoctoral research at FCCC and joined the faculty in 1994. Dr. Adams' research is focused on developing antibody-based molecules to treat and detect cancer. To accomplish this his lab is working to understand the manner by which antibodies target and penetrate into tumors and to use this knowledge to generate antibodies that are more effective at this critical task. His lab is also developing antibodies targeting ovarian, breast and renal cancers and is employing these antibodies as agents to deliver drugs and other agents to sites of tumor in order to increase their efficacy and decrease toxicity to normal tissues. He is also involved in pilot studies to develop novel biosensors (immuno-microcantilevers) to detect cancer and other diseases.

Wei-Heng Shih is a professor in the Department of Materials Science and Engineering at Drexel University. He received a B.Sc. in physics in 1976 from Tsing-Hua University in Taiwan and completed his Ph.D. degree in Physics in 1984 from Ohio State University. After postdoctoral research at University of Washington in Physics department and Materials Science and Engineering department, he joined Drexel University in 1991. His research has covered a wide range of areas of materials science and engineering including surface modification of powders by colloidal coating, sol-gel processing of microporous and mesoporous powders, low-temperature processing of perovskite piezoelectric ceramics, and fabrication of piezoelectric sensors. He has received the American Ceramic society 1999 Edward C. Henry Electronics Division Best Paper Award and the Drexel's Research Achievement Award. His current research focuses on the development of aqueous synthesis of nanocrystalline quantum dots, highly piezoelectric freestanding films, and lead-free piezoelectric ceramics for imaging and sensor applications. He holds the titles of Associated Editor of Journal of the Ceramic Society of Japan, Editorial Board Members of the Journal-Nano Biomedicine and Engineering, and Advisory Member of International Union of Advanced Materials (IUAM).